Kirchhoff imaging as a tool for AVO/AVA analysis [1]

MARTIN TYGEL, LÚCIO T. SANTOS and JÖRG SCHLEICHER, State University of Campinas, UNICAMP, Brazil
PETER HUBRAL, University of Karlsruhe, Germany

Kirchhoff-type weighted stacking methods are used in an ever more sophisticated way with the aim of aggregating amplitude information into imaged seismic sections. This is, for instance, the case of true-amplitude Pre-Stack Depth Migration (PreSDM), in which amplitudes of migrated primary reflections essentially represent a measure of offset-dependent reflection coefficients. Application of true-amplitude PreSDM to several individual common-offset sections give rise to an ensemble of migrated sections directly amenable to an Amplitude-Variations-with-Offset (AVO) analysis.

A more recent time-domain example for Kirchhoff stacking is provided by true-amplitude Migration to Zero Offset (MZO). With this imaging process, common-offset sections are transformed into corresponding simulated zero-offset sections, for which primary reflections have the same geometrical spreading as those that would be measured if an actual zero-offset experiment were performed. At the same time, offset-dependent reflection coefficients are preserved. As zero-offset geometrical-spreading factors can be well estimated from Normal-MoveOut (NMO) velocities, application of true-amplitude MZO to an ensemble of input common-offset input sections, provides an alternative way of estimating offset-dependent reflection coefficients. In this way, true-amplitude MZO sections are also directly amenable to an AVO analysis.

Processing an input section with a second true-amplitude PreSDM or MZO using slightly different weights, leads to the additional determination of the corresponding reflection angles. This means that AVO results can be turned into more informative Amplitude-Variations-with-Angle (AVA) data.

Concerning the above true-amplitude migration and MZO methods for AVO/AVA purposes, it is quite natural to ask about their potential advantages and disadvantages with regards to actual applications. In particular, what are the expected benefits of applying these elaborate algorithms, as op-

[1]Submitted for publication in *The Leading Edge*

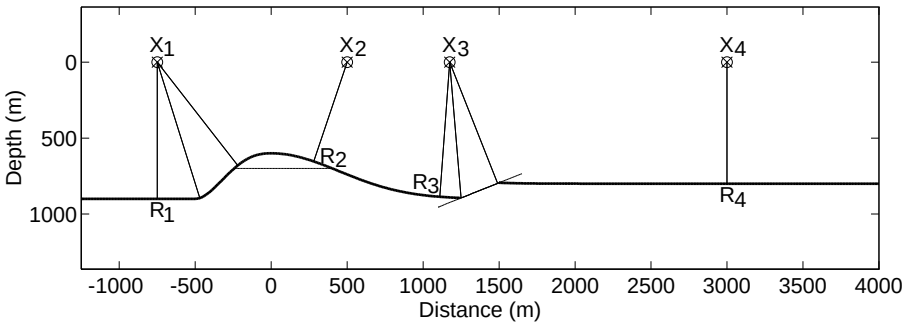

Figure 1: Earth model for the synthetic examples. The AVO and AVA analysis was carried out at the four reflection points R_1 to R_4 that are shown here with their respective normal rays.

posed to, e.g., simple CMP-AVO estimates directly obtained from the CMP gathers?

In practice, time-domain methods, such as MZO, are known to be kinematically less sensitive than depth-domain methods, such as PreSDM, to errors in the given velocity model. However, diffractions and caustics are typical problems in time-domain data that can be better removed by a successful PreSDM. We would intuitively expect an analogous behavior regarding amplitudes.

A classical first approach to check our intuitions and to address the above questions is to examine the performance of the various methods on well-selected and controlled situations. This is done in this paper by means of a simple but illustrative model. The methods of true-amplitude PreSDM and MZO were applied at specific points of a target reflector to compute their AVO/AVA responses. For comparison, we have also considered the routinely applied method of deriving AVO information directly from CMP gathers.

Earth model. Referring to Figure 1, we consider the seismic response of a single, target reflector overlain by a homogeneous acoustic medium of unit density and a velocity of 3.5 km/s. The medium below the reflector is also acoustic and homogeneous with unit density and a velocity of 4.5 km/s, except for a small reservoir zone inside the dome structure, where the velocity assumes the constant value of 2.0 km/s. We have chosen an acoustic Earth

model for reasons of simplicity. Conclusions drawn from this investigation are, for instance, directly applicable to P-P data and even to well-sampled land data with a reproducible source.

The seismic line is a dip line and all point sources are reproducible. The multi-coverage data that are acquired in this way can be modeled and imaged by what is commonly called 2.5-D methods. The attribute 2.5-D refers to the correct consideration of 3-D amplitude effects of in-plane wave propagation in a 2-D medium, i.e., one that does not vary in the out-of-plane direction. The assumption of a 2.5-D situation is well accepted in practice, particularly in the application of MZO and DMO algorithms.

This particular form of the reflector was chosen to study the results of an AVO/AVA analysis at four characteristic points for seismic imaging while leaving all other possible complications out of consideration. Point R_1 lies within a caustic zone due to a strongly curved left flank of the dome. Point R_2 is located above the reservoir, slightly dislocated from its top. Point R_3 is positioned close to a fault where diffractions originate, and point R_4 is a reference point in an unperturbed area on a flat reflector. In spite of its apparent simplicity, the present model contains, in its fundamental form, some of the main structural difficulties faced by all migration and imaging methods when amplitudes are of prime interest.

The multi-coverage reflections from the target reflector are shown in Figure 2a. They were computed by a 2.5-D Kirchhoff-Helmholtz forward modeling algorithm and are displayed in the form of an ensemble of common-offset sections for the offsets $2h = 400$ m to $2h = 2400$ m in steps of $2\Delta h = 100$ m. White noise was added with a signal-to-noise ratio of three with respect to the mean amplitude in the section for $2h = 200$ m. For better visualization, only one common-offset section is displayed in Figure 2a for $2h = 1400$ m. In all common-offset sections, the phenomenon of a caustic to the left of the dome, as well as the phenomenon of diffractions occurring close to the fault are clearly recognizable. The four common-mid-point (CMP) gathers at the CMPs X_1 to X_4 indicated in Figure 1, are explicitly displayed in Figure 3.

Formulation of the problem. Given the multi-coverage data of Figure 2a, a velocity model of the overburden of the target reflector and CMP points X_1 to X_4, to obtain the AVO/AVA responses at the corresponding points R_1 to R_4 at the target reflector.

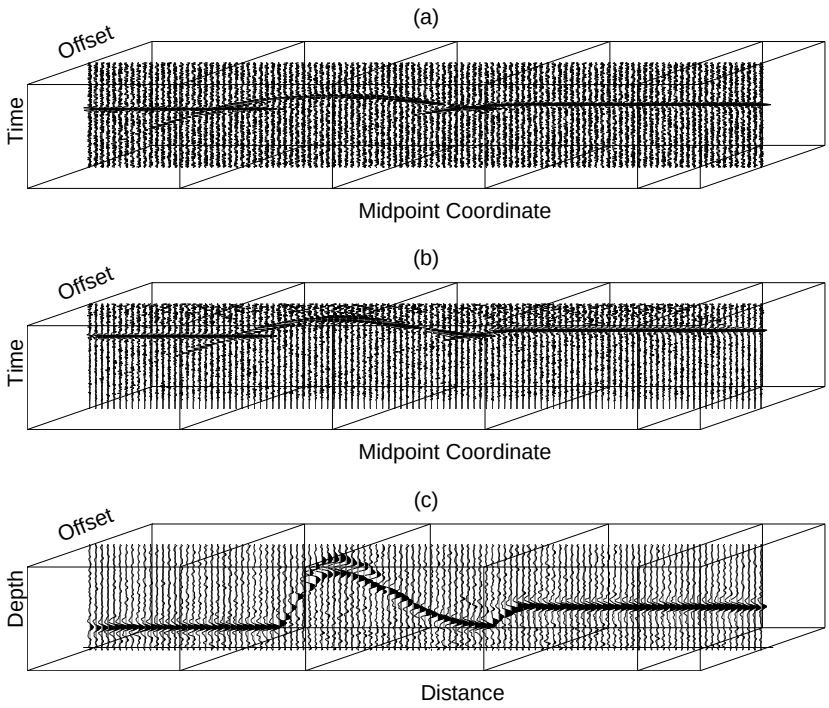

Figure 2: (a) The synthetic data are sorted into common-offset gathers. Here depicted is the one for $2h = 1400$ m. (b) Imaged zero-offset section as a result of true-amplitude MZO applied to the section of Figure 2a. (c) Depth-migrated section as a result of true-amplitude Kirchhoff migration applied to the section of Figure 2a.

Below we present the results of two true-amplitude imaging methods designed to solve the above problem. At first, we show the AVO results obtained using Kirchhoff true-amplitude PreSDM and MZO algorithms, respectively. These are directly compared to the ones obtained by the application of conventional AVO directly on the CMP gather. Thereafter, we show the corresponding AVA results after PreSDM and MZO, respectively.

AVO by true-amplitude PreSDM and MZO. We apply a true-amplitude PreSDM algorithm to an ensemble of individual common-offset sections extracted from the multi-coverage data of Figure 2a. This leads to the corresponding ensemble of common-offset migrated images like the one depicted in Figures 2c. From all migrated common-offset sections, we have

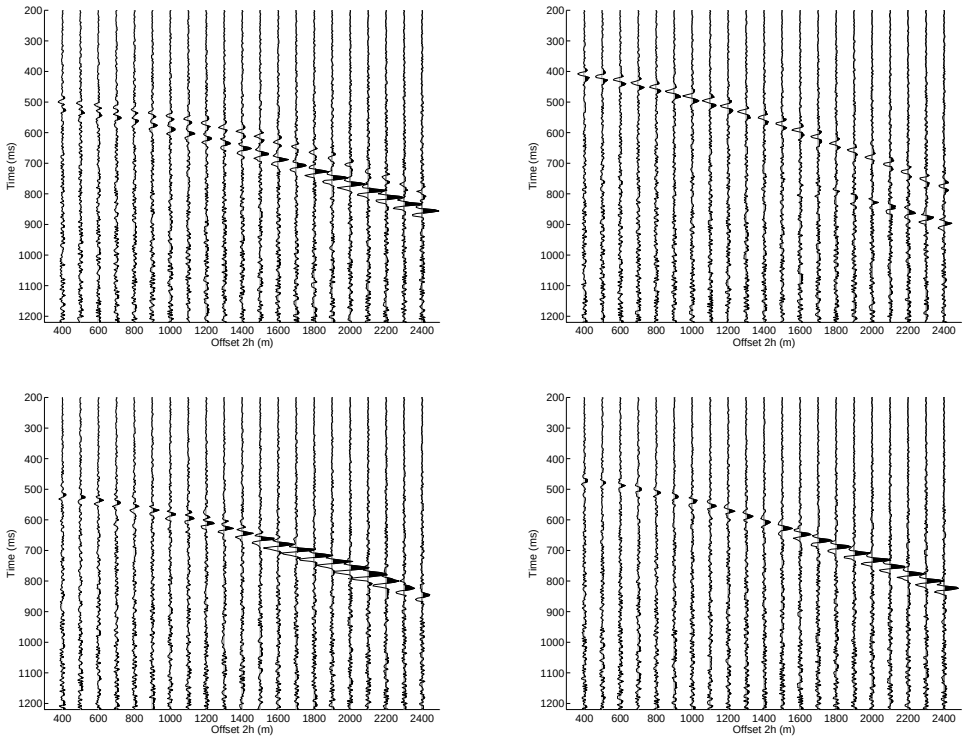

Figure 3: CMP gathers at positions X_1 =-750 m (top left), X_1 =500 m (top right), X_1 =1750 m (bottom left), and X_1 =3000 m (bottom right).

extracted the image gathers of Figure 4 that include the reflector points R_1 to R_4. As a result of the true-amplitude migration, the amplitudes in the image gathers are free from geometrical-spreading losses, thus being a direct measure of the of offset-dependent reflection coefficients. In practice, the true-amplitude output would still suffer from other wave-propagation effects, not removed from the true-amplitude migration algorithm. These include, e.g., attenuation along the ray paths and transmission losses across interfaces. For most AVO purposes, these quantities do not show significant lateral variation, being taken as fixed scaling factors in each image gather. As we are here mainly interested in the differences between AVO/AVA after migration and MZO, we neglect these effects, which would affect migration and MZO in the same way.

We next apply a true-amplitude MZO algorithm to the same ensemble

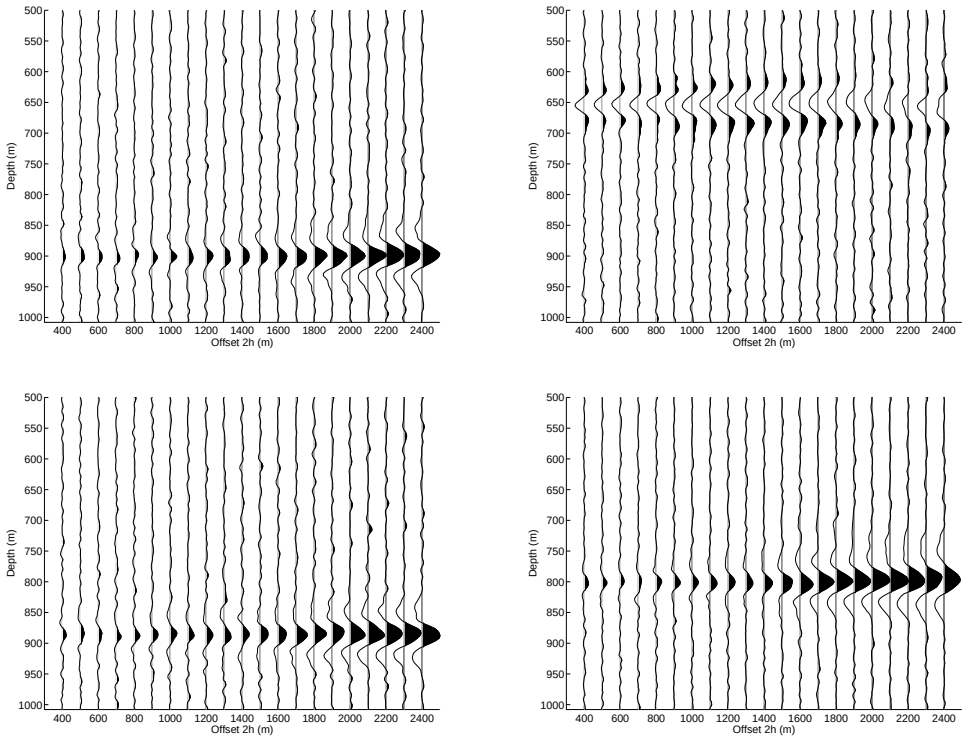

Figure 4: Migrated image gathers at the reflector points R_1 (top left), R_2 (top right), R_3 (bottom left), and R_4 (bottom right).

of individual common-offset sections extracted from Figure 2a. This results in a corresponding ensemble of simulated zero-offset sections like the one shown in Figure 2b. As a result of the application of true-amplitude MZO, simulated zero-offset primary-reflection amplitudes are given by the original offset-dependent reflection coefficients divided by the zero-offset geometrical spreading. The latter can, however, be readily removed using classical formulas based on NMO velocities and zero-offset traveltimes. In the present case of a homogeneous overburden, the geometrical-spreading factor is the product of the overburden (constant) velocity by the zero-offset traveltime. The indicated MZO gathers at the selected CMP points X_1 to X_4 of Figure 2b are displayed in Figure 5.

It should be mentioned that MZO appeared more sensitive to aliasing than PreSDM. The above examples where computed with a trace distance

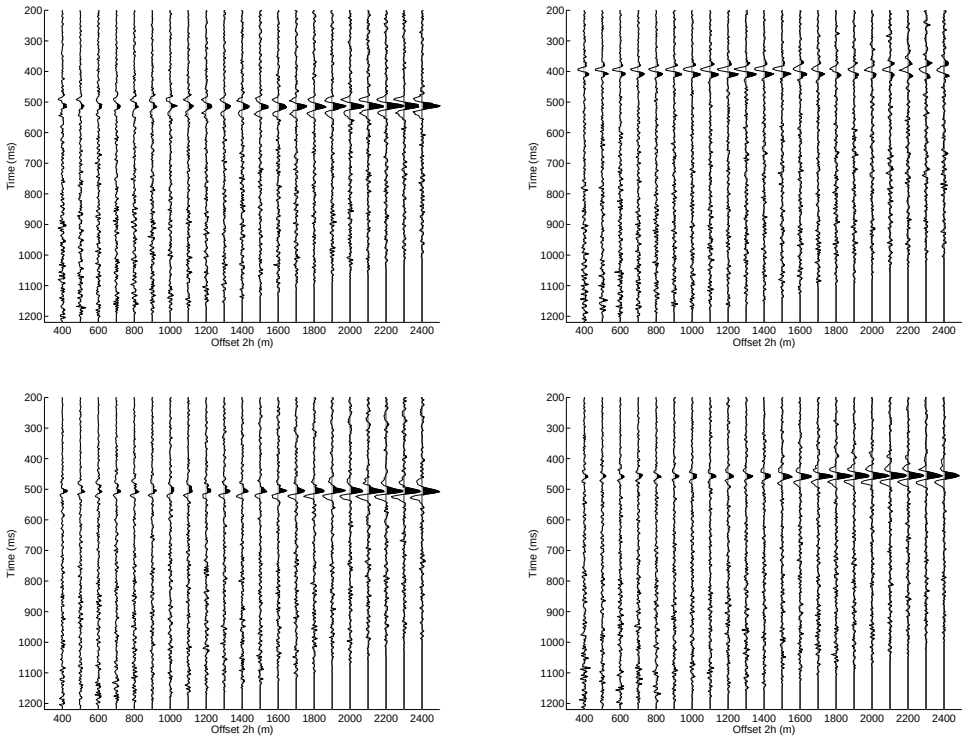

Figure 5: MZO image gathers at the reflector points R_1 (top left), R_2 (top right), R_3 (bottom left), and R_4 (bottom right).

within the common-offset sections of 12.5 m. This close spacing was chosen in order to simulate an amplitude-preserving anti-alias filter. For a trace distance of 25 m, results of PreSDM were not much different, as opposed to the ones of MZO that suffered strongly from aliasing, due to the more steeply dipping flanks of the MZO operator.

AVO analysis. For an AVO analysis, we pick the amplitudes within the CMP section, the MZO image gather and the migrated image gather. To be able to compare the results, the CMP and MZO amplitudes are subjected to the corresponding standard geometrical-spreading correction, i.e., multiplication by traveltime and migration velocity. Plotting the resulting amplitude values as a function of the offset $2h$ for which they were obtained, results in a standard AVO analysis. This is shown in Figure 6 for the four reflector

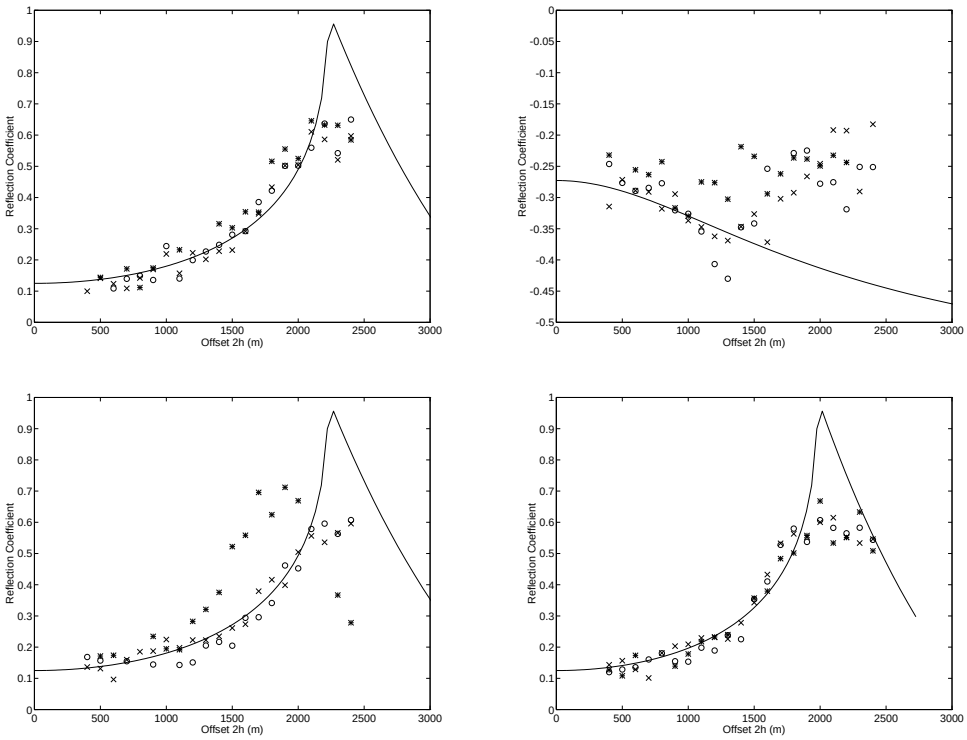

Figure 6: Comparison of amplitudes of CMP (asterisks), MZO (circles), and migration (crosses) with the exact reflection coefficient (solid line) as a function of offset $2h$ at the reflector points R_1 (top left), R_2 (top right), R_3 (bottom left), and R_4 (bottom right).

points R_1 to R_4.

Transforming AVO into AVA. As explained above, reflection coefficients, as a function of offset, can be directly estimated by one application of true-amplitude PreSDM (or MZO). It can be shown, however, that, in addition to the reflection coefficient, the corresponding reflection angle can be also estimated. All that is needed for that purpose is an additional application of the same PreSDM (or MZO) algorithm using slightly different weight functions. By relating the two PreSDM (or MZO) stacking results to each other, one can determine the reflection angle and, thus, one can transform AVO into AVA.

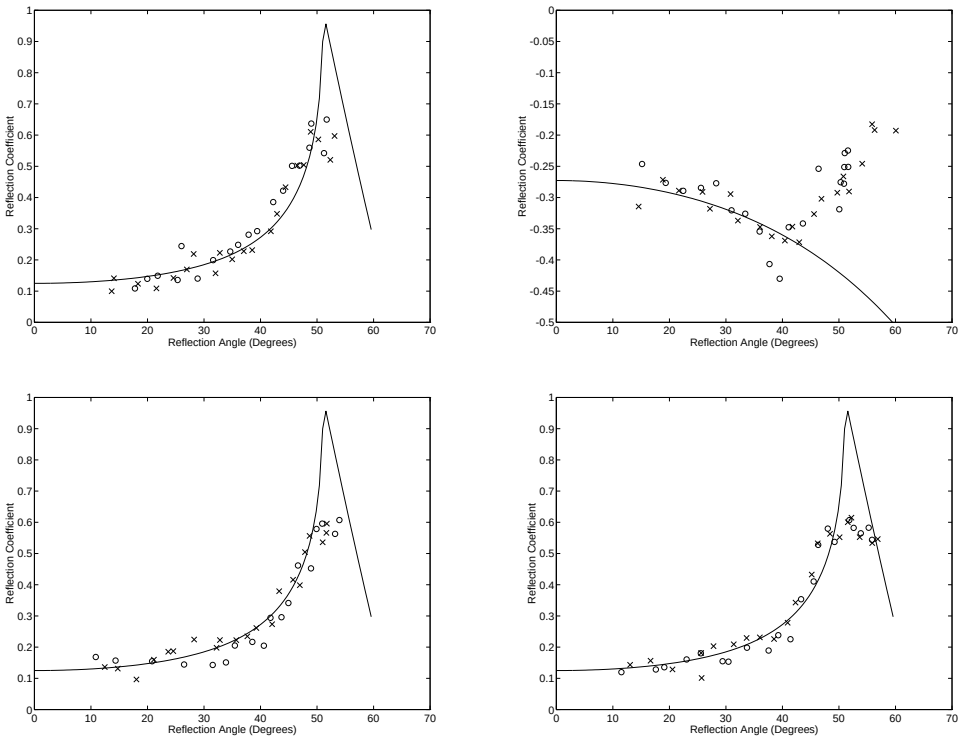

Figure 7: Comparison of amplitudes of MZO (circles) and migration (crosses) as a function of the determined reflection angle with the exact angle-dependent reflection coefficient (solid line) at the reflector points R_1 (top left), R_2 (top right), R_3 (bottom left), and R_4 (bottom right).

AVA analysis. We apply the above-mentioned technique to the previous PreSDM and MZO AVO image gathers of Figure 4 and Figure 5, respectively. The results are the corresponding PreSDM and MZO AVA panels of Figure 7, into which we have superimposed the exact angle-dependent reflection coefficient function directly computed from the model.

Discussion of results. Starting with the simplest situation of point R_4 on the flat and undisturbed part of the target reflector, we observe from the AVO graphs of Figure 6 an excellent agreement between the directly obtained CMP amplitudes with the ones resulting from the application of true-amplitude PreSDM and MZO amplitudes. All values closely match the correct reflection

coefficient. The same is true in the AVA graph of Figure 7 corresponding to PreSDM and MZO data. This indicates that, not only amplitudes, but also angles are extracted very accurately in this simple situation. We may conclude that in such a situation, conventional AVO within the CMP gather is quite sufficient to determine the AVO trend.

Interestingly enough, things do not worsen too much at point R_1, located in the caustic region, as far as PreSDM and MZO are concerned. AVO and AVA analyses yield very good coincidence with the theoretical reflection coefficient. The CMP-AVO gets a little worse than the corresponding results from true-amplitude PreSDM and MZO, but still recovers the AVO trend quite well, although the triplication of events in the bow-tie structure of the caustic is not completely resolved. Note that at some offsets, the asterisks are missing, indicating that the picked value is not within the amplitude range of the figure.

At point R_3, located near the fault, the AVO results differ more clearly. The diffraction events seem to disturb neither the application of the true-amplitude PreSDM nor the MZO algorithm, good results being obtained both in the AVO or AVA domains. However, AVO analysis directly applied to the CMP gather gave rise to considerably worse results, which separate more and more from the true AVO trend for offsets greater than 1100 m.

Finally, at point R_2 located at the top of the low-velocity reservoir zone, we see the most dramatic difference between CMP-AVO and that of true-amplitude PreSDM or MZO. Whereas the latter two remain close to the theoretical curve for about ten offsets, the CMP amplitudes remain so at best for the first five offsets only, thus making an AVO analysis much more difficult. The deviation of all amplitudes from the theoretical curve at larger offsets is due to the larger Fresnel zone, which includes part of the target reflector away from the top of reservoir. The effective velocity below the reflector for these offsets is some weighted mean of the velocities within and outside the reservoir zone.

We observe that in the present model, the velocity contrast along the reflector remains constant, with the exception of the top of reservoir. In a practical situation, in which contrasts may significantly vary along the target reflector, CMP-AVO should be expected to yield accordingly worse results. This is because of the reflection-point smear, namely different reflection points for different offsets. An additional problem with CMP-AVO

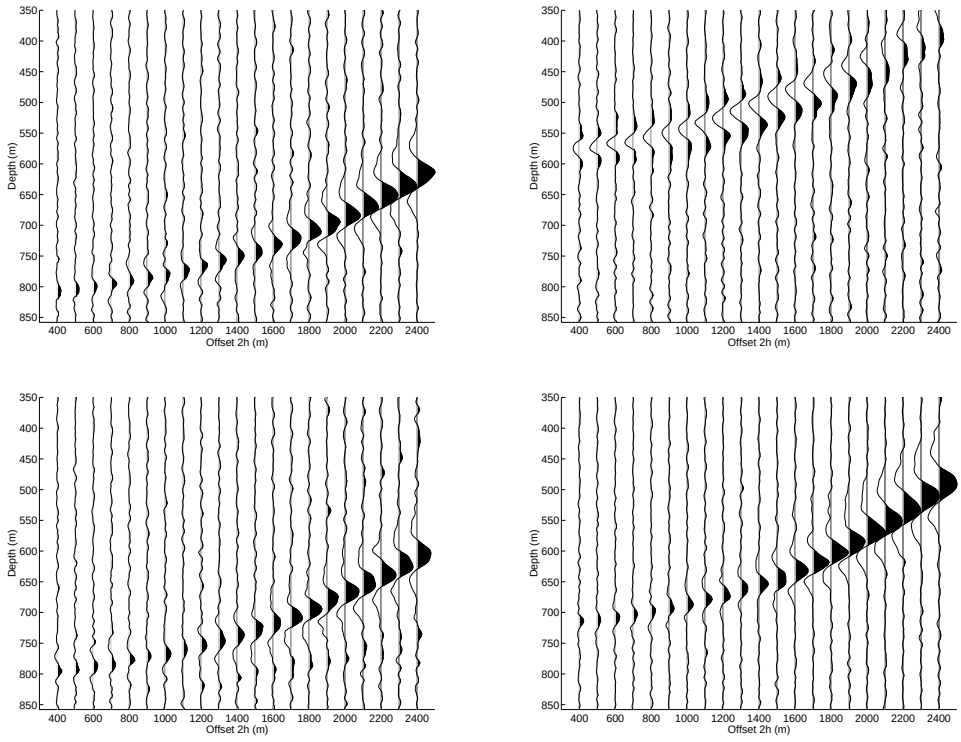

Figure 8: Migrated image gathers at the reflector points R_1 (top left), R_2 (top right), R_3 (bottom left), and R_4 (bottom right) for migration velocity 3.15 km/s.

occurs when the overburden velocity varies, at least with depth. This causes CMP-AVO to result in distorted amplitude estimates at the farther offsets, however not affecting PreSDM and MZO.

Velocity dependence. To study the quality of AVO and AVA analysis in dependence on the migration velocity, we have repeated all the above computations now using the erroneous migration velocity of 3.15 km/s (which is 10 percent too low). Figures 8 and 9 show the respective migrated and MZO image gathers. Comparing Figures 8 with 9, we see that the kinematics of MZO are less affected by the wrong migration velocity than those of PreSDM. The migration error varies between 11% for the smallest offset of $2h = 400$ m and 33% for the largest offset of $2h = 2400$ m, whereas the MZO

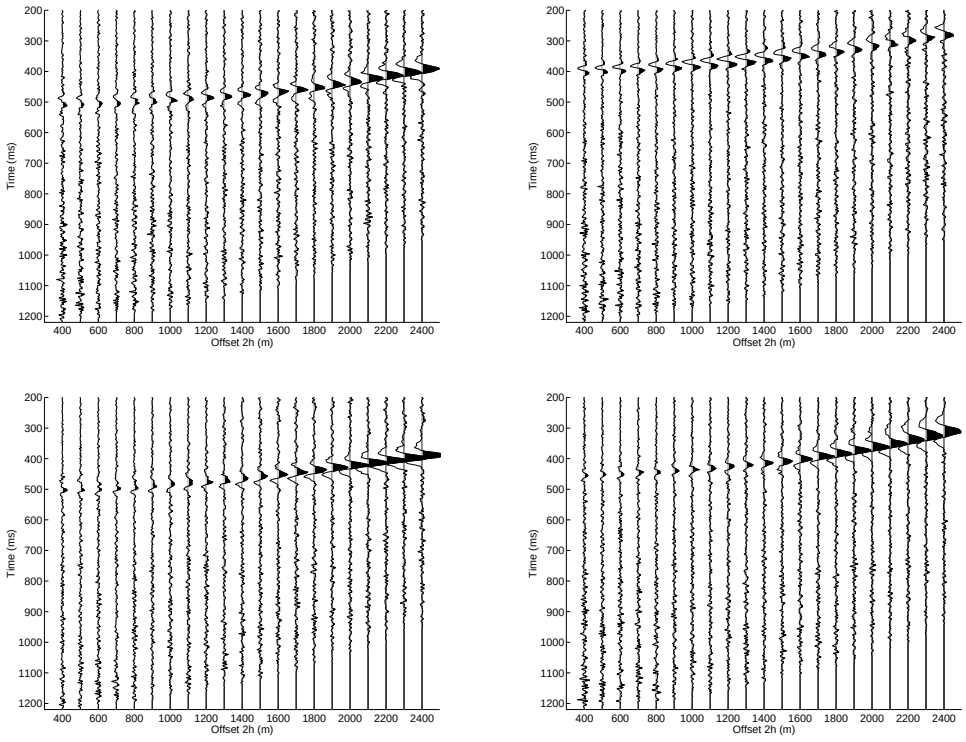

Figure 9: MZO image gathers at the reflector points R_1 (top left), R_2 (top right), R_3 (bottom left), and R_4 (bottom right) for migration velocity 3.15 km/s.

error varies between 0% and 20% only.

Figure 10 shows the corresponding AVO panels. The match between the amplitudes of CMP, MZO as well as migration and the theoretical reflection coefficient remains quite well. As before, at the top-of-reservoir reflection point R_2, the results are worst. Again, migration yields better amplitudes than MZO or CMP. At the other three reflection points, the results of all three methods match the theoretical curve comparably well. The amplitude does not seem to be greatly affected by the incorrect migration velocity. Finally, looking at the AVA graphs in Figure 7 and Figure 11, we observe a shift to larger angles in Figure 11. This is an effect to be expected since, geometrically, a shallower reflector involves larger reflection angles than a deeper one. We conclude that the angle is the quantity most sensitive to velocity

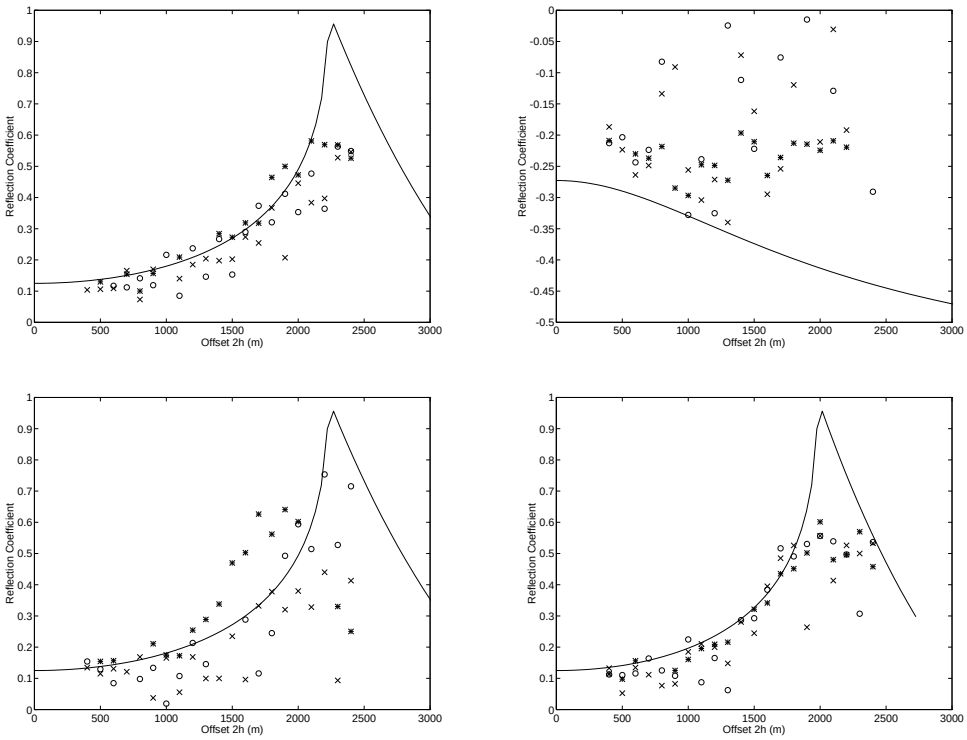

Figure 10: Comparison of amplitudes of CMP (asterisks), MZO (circles), and migration (crosses) with the exact reflection coefficient (solid line) as a function of offset $2h$ at the reflector points R_1 (top left), R_2 (top right), R_3 (bottom left), and R_4 (bottom right) for migration velocity 3.15 km/s.

inaccuracies. However, as one would surely process in practice flat image gathers only, velocity inaccuracies are not expected to be greater than ten percent, such that an AVA analysis remains possible. Comparing the AVO and AVA results of MZO to those of migration, we observe that they present more or less the same stability with respect to migration velocity. Only at supercritical angles, where AVO failed in all of our examples, MZO amplitudes were more strongly affected by the inaccurate velocity than migration amplitudes.

Some comments on AVA inversion. The AVO/AVA analysis described in this paper will be succeeded of course by the inversion of the AVA curves

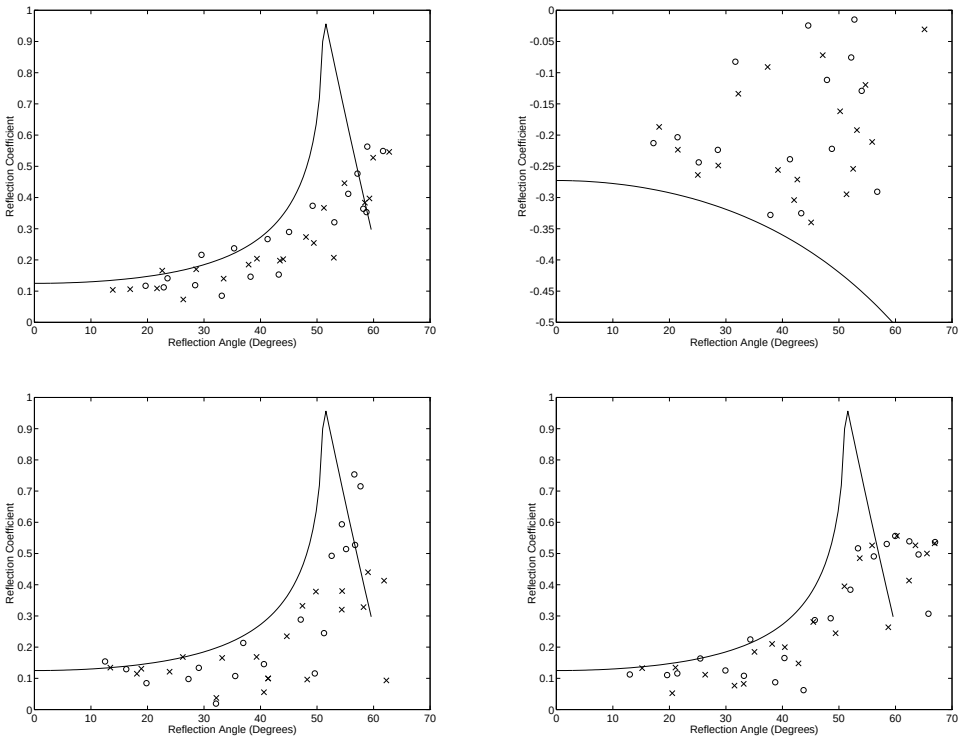

Figure 11: Comparison of amplitudes of MZO (circles) and migration (crosses) as a function of the determined reflection angle with the exact angle-dependent reflection coefficient (solid line) at the reflector points R_1 (top left), R_2 (top right), R_3 (bottom left), and R_4 (bottom right) for migration velocity 3.15 km/s.

with the aim of determining intercept and gradient. Although beyond the scope of this article, let us briefly comment on this inversion. We have carried out, not only a standard inversion of the linearized reflection coefficient for intercept and gradient, but also a nonlinear inversion using the theoretical expression for the acoustic reflection coefficient. The results for the correct migration velocity are quite encouraging, providing almost the exact value for the velocity below the reflector. With exception of the low-velocity reservoir zone, even the errors caused by the use of an incorrectly lower migration velocity were at the expected 10%. The behavior of migration and MZO amplitudes in this respect is more or less the same.

Summary and Conclusions. Having ignored the generally complex overburden of a target reflector in the real Earth, we have, by means of a simple but fundamental example, discussed the application of Kirchhoff-type true-amplitude PreSDM and MZO as tools for an AVO/AVA analysis. The main conclusion to be drawn from our experiments is that both, PreSDM and MZO, are very well suited for this purpose.

The application of true-amplitude PreSDM using the correct reflector-overburden velocity model lead to good results in all situations under consideration. Somewhat contrary to our intuition, true-amplitude MZO has worked equally well even in the vicinity of caustics and diffractions. Also surprising was the fact that PreSDM amplitudes did not suffer more from inaccuracies in the migration velocity than MZO amplitudes. The angle extraction turned out to be significantly more sensitive to migration velocity than the reflection coefficients. This explains the greater errors found in the AVA responses as compared to the corresponding AVO responses.

Although both methods have shown quite similar characteristics and results, some minor differences can be noted. Because of the smaller operator size, MZO is the faster method. In our simple analytic examples, MZO was about a factor two faster than PreSDM. On the other hand, because of the larger operator size, PreSDM has a stronger effect of noise reduction. Also, without an amplitude-preserving anti-aliasing filter, MZO will be more severely affected than PreSDM when applied to field data with insufficient trace spacing.

Our experiments have also confirmed that the simpler and conventional AVO analysis directly applied to the CMP gathers may constitute a reliable method for reflectors along which the velocity contrasts do not significantly vary.

Of course, the present investigation was carried out for a fairly simple Earth model. Additional difficulties will certainly arise when considering a more realistic situation. Nevertheless, we believe that our results indicate the expected behavior of AVO/AVA analysis after true-amplitude PreSDM or MZO in more complex models.

Suggestions for further reading. A general discussion on true-amplitude PreSDM can be found in "True-amplitude seismic migration: A comparison of three approaches" by Gray (*Geophysics*, 1997); for applications of true-

amplitude PreSDM to AVO/AVA see "Why migrate before AVO: a simple example" by Beydoun et al. (1993 EAGE Meeting Abstract), "The impact of migration on AVO" by Mosher et al. (*Geophysics*, 1996) and "3-D AVO migration/inversion of field data" by Tura et al. (*TLE*, 1998); basic descriptions on true-amplitude MZO are given in "2.5-D True-amplitude Kirchhoff migration to zero offset in laterally inhomogeneous media" by Tygel et al. (*Geophysics*, 1998) and in "True-amplitude transformation to zero offset of data from curved reflectors" by Bleistein et al. (*Geophysics*, 1999); the basic ideas on how to transform AVO into AVA using a second application of PreSDM are given in "Imaging reflectors in the earth" by Bleistein, (*Geophysics*, 1987) and "Multiple weights in diffraction-stack migration" by Tygel et al. (*Geophysics*, 1993); the corresponding ideas for true-amplitude MZO are explained in "True-amplitude transformation to zero offset of data from curved reflectors" by Bleistein et al. (*Geophysics*, 1999).

Acknowledgments. We thank Sam Gray for helpful comments and enlightning suggestions. We acknowledge support by CNPq, FAPESP and PRONEX (Brazil), and the sponsors of the WIT Consortium.

Corresponding author. M. Tygel, tygel@ime.unicamp.br